BOND BEHAVIOR OF RIBBED-SURFACE, HEADED-END, GFRP BARS EMBEDDED IN HIGH-STRENGTH CONCRETE

Md Sirajul Islam, Khaled Sennah, Hamdy M. Afefy
Department of Civil Engineering, Ryerson University, Toronto, ON.

Abstract: Glass Fiber Reinforced Polymer (GFRP) bars as a proper substitute for traditional reinforcing steel bars not only eliminate the durability problem due to corrosion of reinforcing steel, but also provide remarkably enhanced capacity due to their high tensile strength compared to that of the steel bars. This paper presents the experimental findings of pullout tests conducted on GFRP bars embedded into high-strength concrete blocks covering different parameters. The studied parameters were bar diameter size, embedment length, bar end condition (headed), and concrete cover to bar. Based on the results of the parametric study, the bond stress was shown to be inversely proportional to the embedment length and bar diameter as expected. In addition, the smaller concrete cover appeared to have significant effect on bond stress, leading to side blow-out failure rather than bar pullout or concrete splitting in the case of headed-end GFRP bars. In addition, the GFRP bar with headed-end showed significant increase in pullout strength compared to that for the straight-end bars. Finally, an empirical expression was proposed to calculate the development length of GFRP bars with headed-end cast in high-strength concrete.

Keywords: bond stress; bar diameter; concrete cover; Glass Fiber Reinforced Polymer (GFRP) bars; headed bars; high-strength concrete; slip.

1 INTRODUCTION

Fiber Reinforced Polymer (FRP) bars have desirable characteristics which give them more advantages over traditional reinforcing steel bars. These characteristics include high tensile strength, corrosive resistance, light weight, electric insulation and fatigue resistance. Hao et al. (2006). Therefore, in the recent years, FRP bars have been introduced as a competent alternative to traditional reinforcing steel bars for different concrete structures subjected to severe environmental conditions such as waste water treatment and chemical plants, floating decks, sea walls and water structures. Benmokrane and Rahman (1998) In addition, it has been found that FRP bars can eliminate durability problem associated with corroded reinforcing bars. However, direct replacement of the reinforcing steel bars with the FRP bars has many concerns due to various differences in the manifested behavior of the two materials under different loading conditions. For instance, FRP exhibits linear elastic behaviour up to failure which means that it exhibits limited ductility. In addition, FRP bars have anisotropic material properties while steel bars have isotropic properties, which make the bond behavior dubious. Furthermore, higher cost of the FRP bars compared to that of steel bars and lack of familiarity with the new technology resulted in slow adaptation of FRP as concrete reinforcement (Okelo and Yuan 2005).

Generally, bond behavior between concrete and reinforcing steel bar can be assumed constant, however this assumption is less valid for GFRP bars due to their relatively lower stiffness compared to that of steel bars. This results in greater slip values at the loaded end than at the free end (Pecce et al. 2001). Thus, the free end slip will be reduced to almost zero once the embedment length is greater than the development length as depicted in Fig. 1(a). Adopting the same concept, the bond stress distribution for headed-ended GFRP bars maybe assumed as shown in Fig. 1(b). Experimental investigations revealed that bond strength of FRP bars increases with decrease in the bar diameter, which is the same results obtained for steel bars. Hao et al. (2006) and Tighiouart et al. (1998) verified that when the diameter of the bar is larger, more bleeding water is trapped beneath the bar. Consequently, there is a greater chance of creating voids around the bar which will eventually decrease the contact surface between the concrete and the bar and thus, reduces bond strength. It was also observed that the maximum average bond stress decreased with an increase in the embedment length as exhibited by steel bars. Due to the nonlinear distribution of the bond stress along the length of the reinforcing bar, as the embedment length increases, the stress is distributed over a longer length and henceforth, the bond strength decreases.

Glass Fiber Reinforced Polymer (GFRP) bars are commonly used in various projects in North America such as bridge deck slabs traffic barrier and parking garages as a substitute of steel reinforcing bars. That is due to their lower cost compared to other types of FRP materials. The current paper presents both experimental and analytical investigations conducted in order to verify the effect of different parameters on the bond characteristics between GFRP bars with headed-end and the surrounding high-strength concrete. In order to increase the reliability of experimental findings, test results of each studied parameter was obtained based on the average results of six identical specimens.

2 EXPERIMENTAL TEST PROGRAM

2.1 Description of the specimens

The test specimens consisted of two sets of GFRP bars. The first set had a bar diameter (d_b) of 12 mm, while the second set had a bar diameter of 16 mm. Table 1 summarizes the geometrical properties for both sizes of the GFRP bars as well as the dimensions of the heads at the bar end depicted in Fig. 1(b).

Table 1 Geometrical properties of the tested GFRP bars

Metric bar size	Core diameter, d_b, mm	External diameter, mm	Cross-sectional area, mm^2	Head length, mm	Head external diameter, mm
12	12	13.5	113	75	28
16	16	18	201	100	40

Table 2 Specimens parameters

d_b, mm	L_{e2} , mm			Head length, mm	Number of identical samples
	0	$4d_b$	$6d_b$		
12	0	48	72	75	6
16	0	64	96	100	6

A total of 108 GFRP bar specimens were tested. Their configurations are shown in Table 2 in accordance with the terminology shown in Fig. 2. Each GFRP bar size had three groups of eccentricity from the specimen edge (concentric, 1.5d_b eccentric and 2.5d_b eccentric, where d_b is the bar diameter) to simulate concrete clear cover to the bar surface. As shown in Figs. 2(a) and (b), the total embedment depth of headed GFRP bars was considered as the head length plus the distance L_e. Three values for L_{e2} were considered in this study, namely: 0, 4d_b and 6d_b. The combinations of the tested parameters resulted in 18 parameters. Accordingly, in order to increase accuracy in experimental results, 6 identical specimens were constructed for each parameter.

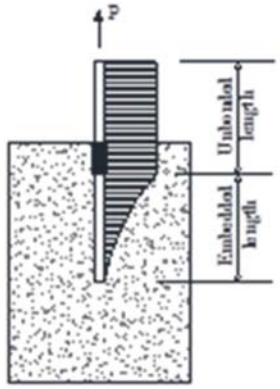

(a) Straight end bar

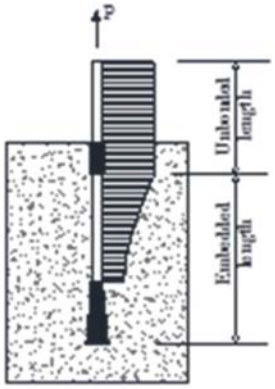

(b) Headed end bar

Fig. 1 Bond stress distribution along a GFRP bar

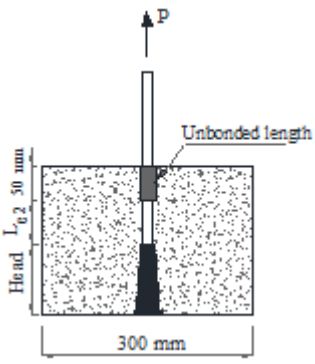

(a) Concentric headed bar

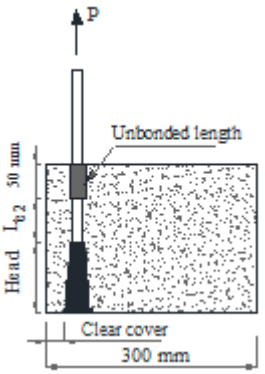

(b) Eccentric headed bar

Fig. 2 Details of test specimens for concentric and eccentric bars

Using plywood, wooden formworks were constructed. The embedment lengths on bars were carefully measured and the unbonded length was covered by regular black electric tape in order to avoid concrete

to touch the bar at the unbonded length. Lumber was later used to construct a support structure providing stability for bars prior to concrete hardening. Figure 3 shows view of the wooden formwork prepared for casting concrete blocks of four parameters. Proper vibration was also provided to avoid air entrapment. Concrete block specimens, while still attached to molding, were cured for few days after casing by placing moist blanket on top of the specimens.

Fig. 3 View of formwork with GFRP bars

(a) Bar shape (b) Headed-end bar (c) Sliced head

Fig. 4 Configurations of the used GFRP bars

2.2 Material properties

2.2.1 Concrete

The used concrete was high-strength ready mix concrete with target concrete cylinder strength of 60 MPa. The test specimens were cast in one day. In order to determine the strength of the concrete, six 100x200 mm concrete cylinders collected from the different locations of the batch were tested after four weeks of curing in the laboratory along with the concrete specimens. The concrete characteristic strength for the concrete was calculated using Eq. 1. Specified in CAN/CSA-S6-06 (2006).

$$[1] \qquad f_c' = 0.9\overline{f_c}\left[1 - 1.28\left[\frac{(k_c V)^2}{n} + 0.0015\right]^{0.5}\right]$$

Where f_c'= concrete characteristic strength; $\overline{f_c}$ = average concrete cylinder strength; k_c = coefficient of variation modification factor for concrete = 1.15 for six samples; *n* = number of concrete cylinder tests = 6; *V* = coefficient of variation of concrete cylinder strengths.

2.2.2 GFRP bars

GFRP bars with ribbed surface supplied by Schöck Canada Inc. (2011) was used in the current study. Two different bar diameters of 12 and 16 mm were used in this study as illustrated in Fig. 4(a). The anchor head material is a thermo-setting polymeric concrete made from high strength concrete mix and vinylester resin, which is then injected into a two part tool that wraps around the bar end. High temperature (95 degree) and pressure (6 bar) are applied until the anchor head is cured to the bar. The maximum outer diameter of the end heads is 2.5 times the diameter of the bar. The head lengths of the 16 and 12 mm diameter bars are 100 and 75 mm long, respectively as given in Table 2. It begins with a wide disk which transfers a large portion of the load from the bar into the concrete. Beyond this disk, the head tapers in five steps to the outer diameter of the blank bar. This tapered geometry ensures optimal anchorage forces and minimal transverse splitting action in the vicinity of the head as shown later in the experimental findings.

2.3 TEST SETUP, TEST PROCEDURE AND INSTRUMENTATION

The type of pullout testing undertaken in this research is called confined pullout testing, since the top of concrete is under bearing compression from the bearing plate. This would prevent concrete cones to form on top of concrete at failure. S807-10 (2010) The main requirement specified in CSA-S807 standard S807-10 (2010) for this type of testing is that the grip distance should be at least $40d_b$, where d_b is the bar

diameter. This limitation was considered in all test setups. In addition, all pullout tests were performed according to the S806-02. CAN/CSA S806-02 (2002) test equipment and requirements.

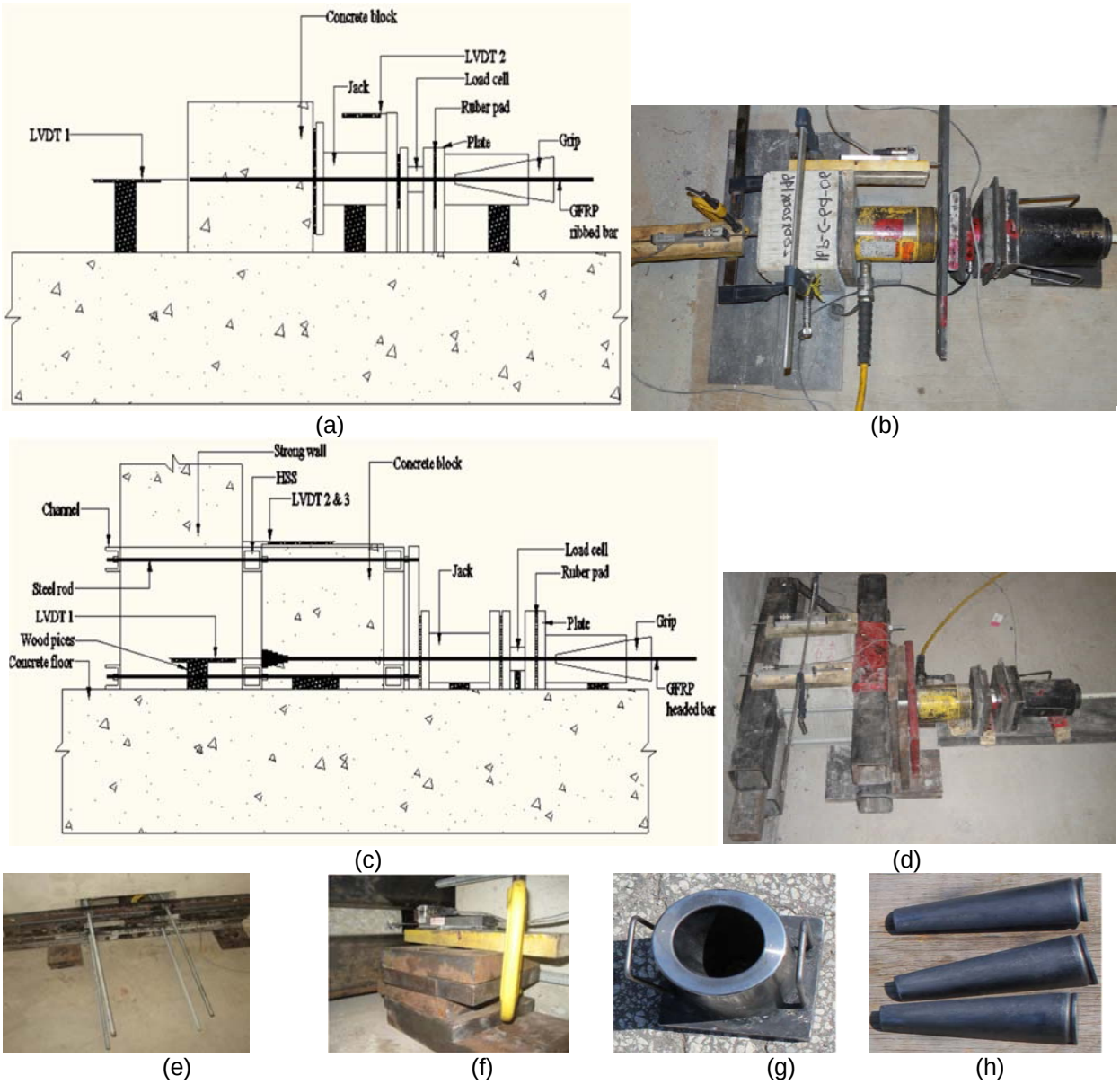

Fig. 5 Test setup: (a) Schematic diagram of the test setup for the concentric pullout testing; (b) View of the test setup for concentric bar testing; (c) Schematic diagram of the test setup for the eccentric pullout testing; (d) View of front side of the test setup for eccentric bar testing; (e) View of back side of the setup for eccentric bar test; (f) View of the potentiometers at back side of the concrete cube for eccentric bar test; (g) Views of the steel grip cylinder and (h) View of the wedges used in the anchorage system.

Two test setups were designed and assembled to apply tensile force on the GFRP bars at their free ends. The first setup was designed for concentric specimens, while the second one was designed for eccentric specimens. A custom-made grip that was designed for pullout testing of ribbed-surface GFRP bars and was used to perform pullout testing is shown in Fig. 5(g) and (h). It consists of a steel cylinder with inner conical hollow shape. It has two handles to carry it as shown in Fig. 5(g). To grip the bar, three wedges with threads were manufactured for each bar diameter. First, the grip cylinder should be placed while the GFRP bar is projecting from the middle of the cylinder. Then, three wedges were inserted in the cylinder.

After assembling the test setup, the pullout test was performed by applying the pullout load at a specified rate using the hydraulic jack operated in an open loop control. The load was applied to the GFRP bar at a rate not greater than 22 kN/min, while the free end slip was recorded with an accuracy of 0.001 mm [50]. The data from the load cell and potentiometers were recorded using test control software (TCS) with a data acquisition unit. The data acquisition system recorded the applied load with a precision of 0.01 kN. According to the S806-02 pullout test requirements, the test was terminated when one of the following conditions occurred: (a) the FRP bar ruptured; or (b) FRP bar slipped a distance at least equal to its diameter. Tables 3 and 4 present test parameters and associated specimen descriptions. The specimen nomenclature consists of 4 symbols separated by a dash. The first symbol indicates the bar size and type of bar (12H = 12 mm headed end, 16H = 16 mm headed end). The second nomenclature stands for concrete cover configuration (C = concentric, E1.5 = eccentricity or clear concrete cover equal to 1.5 times the bar diameter, E2.5 = eccentricity or clear concrete cover equal to 2.5 times the bar diameter). The third term in bar designation specifies the Le2 embedment lengths shown in Fig. 2 in terms of the bar diameter d (e.g. 4d means that Le2 are equal to 4 times the bar diameter). The fourth symbol in the designation indicates the number of identical specimen in the group, ranging from 01 to 06 since there are six identical specimens in total. For instance, 12H-C-0d-01 can be interpreted as follows: 12H = 12 mm headed bar; C = the eccentricity type is concentric; 0d = embedment length consists of the head length where Le2 = 0; and 01 = specimen number 1 in the group.

3 RESULTS AND DISCUSSIONS

In this section, the influence of different parameters on the mode of failure is investigated. Seven types of failure were observed for headed-end GFRP bars as shown in Fig. 6. In pullout failure, the bar was pulled out of the specimen without any splitting/cracking in the concrete as illustrated in Fig. 6(a). In the concrete block-split, crack that started in the smallest cover propagated through the whole concrete block as illustrated in Fig. 6(b). In bar rupture, the bar ruptured when its tensile strength was exhausted as illustrated in Fig. (c). In side blow-out failure, the concrete part in the smaller cover side was blowed-out as depicted in Fig. 6(d). In cover failure, a crack in the smallest cover was suddenly formed, with immediate loss of bond resistance leading to separation of the GFRP bar from the concrete block as depicted in Fig. 6(e). In the diagonal concrete cover failure and due to the lack of homogeneity of the concrete, the developed cover cracks deviated in the lateral direction in the case of eccentric configuration as depicted in Fig. 6(f). Finally, in the V-shaped cover failure, this mode of failure is similar to the pervious one except that failed concrete cover takes the V-shape as depicted in Fig. 6(g). In summary, for headed-end bars, the concrete cover has to be sufficient enough in order to be able to eliminate the concrete cover failure. In addition, bar size can affect or detain the concrete block-split failure mode where the concrete block-split failure was developed mainly by the 16 mm diameter bars. For the 12 mm diameter straight bars, the clear concrete cover of $1.5d_b$ was enough to ensure pure pullout failure, whereas for the 16 mm straight-end bars, the same concrete cover ($1.5d_b$) was not enough to prevent cracking. However, considering all studied parameters, the main failure mode was pure bar pullout, which represented about one third of the total number of the tested specimens.

(a)Bar pullout (b) Concrete block-split (c)Bar rupture (d)Concrete side blow-out (e) Concrete cover failure (f) Diagonal concrete cover failure (g) V-shaped concrete cover failure

Fig. 6 Typical modes of failures observed experimentally

In the current study, the characteristic tensile loads are used instead of average failure loads in order to account for the variation of the actual tensile loads for each specimen. According to S807-10 (2010), the characteristic load can be calculated using Eq. 2.

$$[2] \qquad F_t = \left(\frac{1 - 1.645V}{1 + \frac{1.645V}{\sqrt{n}}}\right).F_{av}$$

Where F_t = the characteristic failure load; F_{av} = the average failure load; n = number of identical samples = 6; V = coefficient of variation of failure loads.

The average bond stress along the embedded length for each specimen was calculated using Eq. 3.

$$[3] \qquad \tau = \frac{F}{\pi d_b h_e}$$

Where, τ =average bond stress (MPa); F = applied load (N); d_b = bar diameter (mm) and h_e = embedment length considering the head length as given in Table 2 (mm).

For the headed-end GFRP bars, the embedment lengths consisted of the length L_{e2} as illustrated in Fig. 2 and their values are given in Table 2 in addition to the head length as given Table 1. Thus, by summation and these two lengths for both bar diameters are then divided by the bar diameter, the embedment lengths for both bar diameters are 6.25d_b, 10.25d_b and 12.25d_b, respectively. Figure 7 depicts the effect of the embedment length on the average bond stress for headed-end bars of both 12 and 16 mm diameter corresponding to different concrete covers. It is worth mentioning that the second symbol in the specimen designation corresponding to the concrete cover as a multiplier of the bar diameter. It can be observed that the average bond stress decreases with increase in the embedment length for headed-end bars for either 12 or 16 mm bar diameter. It can be noted from reported results in Tables 3 and 4 that the average failure load increases by increasing the embedment length, however the corresponding bond stress decreases as illustrated by Eq. 3.

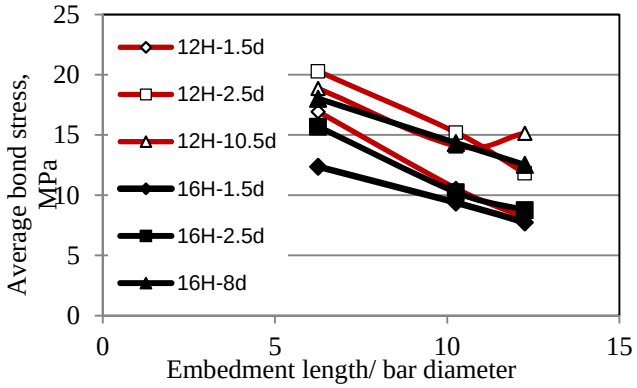

Fig. 7 Relationship between the embedment length/ Bar diameter for all specimens and the corresponding average bond stress

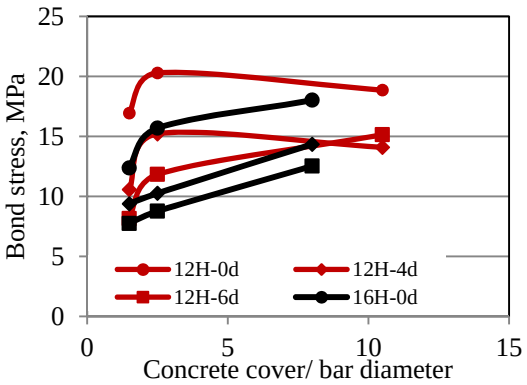

Fig. 8 Relationship between the concrete cover /bar diameter for all specimens and the corresponding average bond stress

Table 3 Test result for 12 mm GFRP bars with headed ends

Parameter #	Test No.	Specimen description	Failure load, kN	Average failure load, kN (5)	Coefficient of variation (COV)	Characteristic load, kN based on S807-10 (7)	(7)/ (5)	Mode of failure
1	1	12H-C-0d-01	77.45	70.54	0.113	53.36	0.76	Bar pullout
	2	12H-C-0d-02	60.12					Bar pullout
	3	12H-C-0d-03	64.14					Bar pullout
	4	12H-C-0d-04	76.53					Bar pullout
	5	12H-C-0d-05	66.28					Bar pullout
	6	12H-C-0d-06	78.74					Bar pullout
2	1	12H-E1.5d-0d-01	75.15	66.99	0.134	47.88	0.71	Side blow-out
	2	12H-E1.5d-0d-02	78.91					Bar pullout
	3	12H-E1.5d-0d-03	60.25					Cover failure
	4	12H-E1.5d-0d-04	68.39					Concrete block split
	5	12H-E1.5d-0d-05	55.14					Cover failure
	6	12H-E1.5d-0d-06	64.12					Cover failure
3	1	12H-E2.5d-0d-01	76.23	69.95	0.082	57.34	0.82	Cover failure
	2	12H-E2.5d-0d-02	68.55					Cover failure
	3	12H-E2.5d-0d-03	60.31					Cover failure
	4	12H-E2.5d-0d-04	68.84					V-shaped cover failure
	5	12H-E2.5d-0d-05	70.40					V-shaped cover failure
	6	12H-E2.5d-0d-06	75.34					Cover failure
4	1	12H-C-4d-01	115.04	96.03	0.152	65.28	0.70	Bar rupture
	2	12H-C-4d-02	87.93					Bar pullout
	3	12H-C-4d-03	82.59					Bar pullout
	4	12H-C-4d-04	95.19					Bar rupture
	5	12H-C-4d-05	82.60					Bar pullout
	6	12H-C-4d-06	112.8					Bar rupture
5	1	12H-E1.5d-4d-01	53.75	71.22	0.148	48.96	0.69	Diagonal concrete cover
	2	12H-E1.5d-4d-02	67.55					Side blow-out
	3	12H-E1.5d-4d-03	80.30					Cover failure
	4	12H-E1.5d-4d-04	69.39					Side blow-out
	5	12H-E1.5d-4d-05	72.80					Cover failure
	6	12H-E1.5d-4d-06	83.50					Cover failure
6	1	12H-E2.5d-4d-01	89.61	84.87	0.077	70.52	0.83	Cover failure
	2	12H-E2.5d-4d-02	84.70					Concrete block split
	3	12H-E2.5d-4d-03	91.10					Bar pullout
	4	12H-E2.5d-4d-04	80.20					Cover failure
	5	12H-E2.5d-4d-05	74.38					Bar pullout
	6	12H-E2.5d-4d-06	89.20					Diagonal concrete cover
7	1	12H-C-6d-01	94.53	98.40	0.067	83.83	0.85	Bar rupture
	2	12H-C-6d-02	108.35					Bar rupture
	3	12H-C-6d-03	90.59					Bar rupture
	4	12H-C-6d-04	94.15					Bar rupture
	5	12H-C-6d-05	99.79					Bar pullout
	6	12H-C-6d-06	102.98					Bar rupture
8	1	12H-E1.5d-6d-01	66.40	73.24	0.186	45.23	0.62	Side blow-out
	2	12H-E1.5d-6d-02	96.23					Cover failure
	3	12H-E1.5d-6d-03	73.59					Bar pullout
	4	12H-E1.5d-6d-04	56.59					Diagonal concrete cover
	5	12H-E1.5d-6d-05	67.32					Side blow-out
	6	12H-E1.5d-6d-06	79.29					Side blow-out
9	1	12H-E2.5d-6d-01	103.00	92.79	0.138	65.56	0.71	Cover failure
	2	12H-E2.5d-6d-02	84.69					Cover failure
	3	12H-E2.5d-6d-03	84.53					Bar pullout
	4	12H-E2.5d-6d-04	86.76					Bar pullout
	5	12H-E2.5d-6d-05	83.43					Bar pullout
	6	12H-E2.5d-6d-06	114.30					Bar rupture

Table 4 Test result for 16 mm GFRP bars with headed ends

Parameter #	Test No.	Specimen description	Failure load, kN	Average failure load, kN (5)	Coefficient of variation (COV)	Characteristic load, kN based on S807-10 (7)	(7)/(5)	Mode of failure
10	1	16H-C-0d-01	142.67	123.11	0.124	90.57	0.74	Bar rupture
	2	16H-C-0d-02	107.84					Concrete block split
	3	16H-C-0d-03	123.94					Concrete block split
	4	16H-C-0d-04	136.87					Concrete block split
	5	16H-C-0d-05	122.99					Concrete block split
	6	16H-C-0d-06	104.36					Concrete block split
11	1	16H-E1.5d-0d-01	80.31	94.16	0.163	62.13	0.66	Concrete block split
	2	16H-E1.5d-0d-02	83.50					Concrete block split
	3	16H-E1.5d-0d-03	113.70					Concrete block split
	4	16H-E1.5d-0d-04	110.50					Concrete block split
	5	16H-E1.5d-0d-05	97.38					Concrete block split
	6	16H-E1.5d-0d-06	79.59					Concrete block split
12	1	16H-E2.5d-0d-01	103.27	113.31	0.144	78.82	0.70	Concrete block split
	2	16H-E2.5d-0d-02	132.60					Concrete block split
	3	16H-E2.5d-0d-03	120.50					Concrete block split
	4	16H-E2.5d-0d-04	97.07					Concrete block split
	5	16H-E2.5d-0d-05	96.69					Concrete block split
	6	16H-E2.5d-0d-06	129.70					Concrete block split
13	1	16H-C-4d-01	140.11	152.17	0.103	118.12	0.78	Bar rupture
	2	16H-C-4d-02	147.91					Bar rupture
	3	16H-C-4d-03	138.09					Bar rupture
	4	16H-C-4d-04	157.31					Bar rupture
	5	16H-C-4d-05	148.53					Bar rupture
	6	16H-C-4d-06	181.04					Bar rupture
14	1	16H-E1.5d-4d-01	91.54	106.13	0.127	77.40	0.73	Side blow out
	2	16H-E1.5d-4d-02	109.73					Concrete block split
	3	16H-E1.5d-4d-03	98.21					Side blow out
	4	16H-E1.5d-4d-04	130.20					Side blow out
	5	16H-E1.5d-4d-05	107.00					Side blow out
	6	16H-E1.5d-4d-06	100.07					Concrete block split
15	1	16H-E2.5d-4d-01	126.60	128.73	0.165	84.55	0.66	Concrete block split
	2	16H-E2.5d-4d-02	109.42					Concrete block split
	3	16H-E2.5d-4d-03	122.63					Concrete block split
	4	16H-E2.5d-4d-04	105.51					Concrete block split
	5	16H-E2.5d-4d-05	153.72					Side blow out
	6	16H-E2.5d-4d-06	154.52					Side blow out
16	1	16H-C-6d-01	161.31	145.95	0.070	123.40	0.85	Bar rupture
	2	16H-C-6d-02	153.53					Bar rupture
	3	16H-C-6d-03	140.34					Bar rupture
	4	16H-C-6d-04	145.69					Bar rupture
	5	16H-C-6d-05	132.50					Bar rupture
	6	16H-C-6d-06	142.32					Bar rupture
17	1	16H-E1.5d-6d-01	125.46	119.41	0.174	76.26	0.64	Side blow out
	2	16H-E1.5d-6d-02	101.98					Side blow out
	3	16H-E1.5d-6d-03	142.46					Side blow out
	4	16H-E1.5d-6d-04	99.45					Side blow out
	5	16H-E1.5d-6d-05	102.82					Side blow out
	6	16H-E1.5d-6d-06	144.30					Side blow out
18	1	16H-E2.5d-6d-01	156.12	137.28	0.179	86.34	0.63	Bar rupture
	2	16H-E2.5d-6d-02	172.99					Bar rupture
	3	16H-E2.5d-6d-03	110.11					Concrete block split
	4	16H-E2.5d-6d-04	117.31					Concrete block split
	5	16H-E2.5d-6d-05	144.54					Concrete block split
	6	16H-E2.5d-6d-06	122.61					Concrete block split

Figure 8 depicts the effect of the concrete cover on the average bond stress for headed-end bars of either 12 or 16 mm diameter corresponding to different embedment lengths. For headed-end bars, the 16 mm diameter bars showed increased average bond stress with increase in the concrete cover from $1.5d_b$ to $2.5d_b$, while these increases showed lower rate moving to concrete cover of $8d_b$. On the other hand, the 12 mm diameter bars showed slight increase beyond concrete cover of $2.5d_b$. For headed-end bars, the average bond stresses corresponding to the lowest embedment length showed the highest values for

both 12 and 16 mm bar diameters. It can be concluded that a concrete cover of 2.5d_b is sufficient in order to provide enhanced bond stress without concrete cover failure since the concrete cover provides confinement to the bars which increases the bond strength (Ehsani et al. 1993). Based on reported results in Table 5, there is an increase in failure load capacity with increase in bar diameter from 12 to 16 mm in all cases of headed-end bars. The failure load of specimens with 6d_b embedment depth is much more than those with 4d_b embedment depths. However, the corresponding bond stress decreased with increase in the bar diameter where such increases in the ultimate loads were accompanied by higher embedment length. Even at the same embedment length, the increases in the ultimate loads could not compensate the decreases in the bond stress due to larger bar diameter values in the denominator of Eq. 3. The test results assured that increasing the bar diameter lowers the bond strength of the GFRP bars.

Table 5 Average failure loads and corresponding bond strength for the tested specimens

Bar diameter mm	End type	Embedment length		Concrete cover		Average failure Load (kN)	Characteristic load, kN based on S807-10	(8)/(7)	Average bond strength MPa	Average slip at maximum load, mm
		Times *d*	mm	Times *d*	mm	(7)	(8)			
12	Headed	0*d*	75	1.5*d*	18	66.99	47.88	0.71	16.94	0.21
				2.5*d*	30	69.95	57.34	0.82	20.29	0.16
				10.5*d*	143	70.54	53.3	0.76	18.86	0.11
		4*d*	123	1.5*d*	18	71.22	48.96	0.69	10.57	0.14
				2.5*d*	30	84.87	70.52	0.83	15.21	0.12
				10.5*d*	143	96.03	65.28	0.68	14.09	0.06
		6*d*	147	1.5*d*	18	73.24	45.23	0.62	8.16	0.12
				2.5*d*	30	92.79	65.56	0.71	11.83	0.11
				10.5*d*	143	98.40	83.83	0.85	15.14	0.04
16	Headed	0*d*	100	1.5*d*	24	94.16	62.13	0.66	12.37	0.16
				2.5*d*	40	113.31	78.82	0.70	15.69	0.11
				8*d*	141	123.11	90.57	0.74	18.02	0.08
		4*d*	164	1.5*d*	24	106.13	77.40	0.73	9.39	0.10
				2.5*d*	40	128.73	84.55	0.66	10.26	0.09
				8*d*	141	152.17	118.12	0.78	14.34	0.05
		6*d*	196	1.5*d*	24	119.41	76.26	0.64	7.74	0.07
				2.5*d*	40	137.28	86.34	0.63	8.77	0.06
				8*d*	141	145.95	123.4	0.85	12.53	0.03

Since previous studies indicated that good correlation exists between the bond strength and the square root of the compressive strength of concrete besides the bond stress is inversely proportional to the bar diameter size, Eq. (3) cab be rewritten in the following form to obtain bar development length.

[4] $$l_d = B\frac{d_b f_t}{\sqrt{f_c'}}$$

Where, f_c'= concrete compressive cylinder strength (MPa) and constant B can be determined based on experimental results based on the following equation and the experimental bond strength values in Table 5.

[5] $$B = \frac{d_b}{4A} = \frac{\sqrt{f_c'}}{4\tau}$$

In order to enable these bars to exhaust their design tensile strength, the embedment lengths had to increase as manifested by the comparison between the embedment length and the development length. For headed-end bars, the actual tensile stresses were higher than the design values. This means the provided bar heads enabled the GFRP bars to use their design tensile stresses where the head length

only without additional embedment length was sufficient to reach the design tensile strength of the GFRP bars. Based on the calculated values, the constant *B* should be selected in such a way that the resulting equation yields a conservative value of the development length. Consequently, constant *B* used in Eq. (4) can be suggested as follows based on experimental findings in Table.

[6] $B = 0.13 + \frac{l_{e2}}{80\, d_b}$ (For headed-end bars)

Where l_{e2}= the additional straight part of the bar to the head as a multiplier of the bar diameter. Thus, the development length for headed-end, ribbed-surface, GFRP bars embedded in high-strength concrete can be proposed as follows:

[7] $l_d = \left(0.13 + \frac{l_{e2}}{80 d_b}\right).\frac{d_b.f_t}{\sqrt{f_c'}}$ (Headed-end bars)

4. CONCLUSIONS

The effect of different parameters on the bond behavior of headed-end, ribbed-surface, GFRP bars embedded in high-strength concrete was studied experimentally on 108 pullout test specimens. These parameters included bar diameter, embedment length, and concrete cover. Results showed that the average failure load increased by increasing the embedment length. Due to different concrete splitting mechanisms, there was not much difference between splitting force obtained for various embedment depths in each case. This is due to the stress concentration around the bars' head which is similar in specimens with various embedment lengths having the same concrete cover. On the other hand, increasing the embedment length led to a decrease in the corresponding bond stress. As the concrete cover increased, the amount of confinement provided by concrete increased and, as a result, the failure load increased in majority of cases along with increasing the corresponding bond stress. Increasing concrete cover further than 2.5d_b for both the 12 and 16 mm diameter bars did not result in noticeable increase in bond stress. This means that concrete cover of 2.5d_b can provide enough confinement to prevent premature concrete cover failure. Increasing bar size showed significant increase in the ultimate load, while the corresponding bond stress decreased in all cases. Although, these increases in the ultimate load increased with increased embedment length, the corresponding bond stresses were decreased. Significant increases in both the ultimate load and the bond stress for all embedment lengths and concrete cover values. Based on experimental findings, an empirical expression of the development length of ribbed-surface GFRP bars cast in high-strength concrete was deduced.

REFERENCES

Aly., R., Benmokrane, B,. and Ebead, U. 2006. Tensile lap splicing of fiber-reinforced polymer reinforcing bars in concrete. ACI Structural Journal, 103: 857-864.

Benmokrane, B., Rahman, H. 1998. Durability of fiber reinforced polymer (FRP) composites for construction. Proceedings of the 1st International Conference (CDCC '98), Québec, Canada.

CAN/CSA-S6-06. 2006. Canadian Highway Bridge Design Code. Canadian Standards Association, Toronto, Ontario, Canada.

Hao, Q., Wang, B., and Ou J. 2006. Fibre reinforced polymer rebar's application to civil engineering. Concrete Journal, 9: 38-40.

Okelo, R., and Yuan, R. 2005. Bond strength of fibre reinforced polymer rebars in normal strength concrete. Journal of Composites for Construction, 9: 203-213.

Pecce, M., Manfredi, G., Realfonzo, R., and Cosenza, E. 2001. Experimental and analytical evaluation of bond properties of GFRP bars. Journal of Materials in Civil Engineering, 13: 282-290.

Schoeck Canada Inc. 2011. Schöck ComBAR Technical Information. www.schöckcanada.ca.

S807-10. 2010. Specification for fiber-reinforced polymers, Canadian Standard Association. Toronto, Ontario, Canada.

Tighiouart, B., Benmokrane, B., and Gao, D. 1998. Investigation of bond in concrete member with fibre reinforced polymer (FRP) bars. Journal of Construction and Building Materials, 12: 453-462.